DAΦNE TECHNICAL NOTE

INFN - LNF, Accelerator Division

Frascati, March 28, 1996

Note: **L-23**

QUADRUPOLE MODELLING

C. Biscari

Optical linear properties of quadrupoles are usually described in the rectangular model approximation, in which the first order transport matrix is defined by the magnetic length of the quadrupole and by its gradient. This is a very good approximation as long as the ratio between the bore radius and the magnetic length is small. As this ratio increases the field gradient longitudinal behaviour cannot be approximated by a rectangle and the description by the usual matrix is not sufficiently accurate. The deviation of the effective linear transport matrix from the rectangular model increases with the gradient value. A discussion of these deviations for the different types of quadrupoles in DAΦNE is given in the following.

DAΦNE Main Ring Quadrupoles

In the DAΦNE Main Rings there are eight types of quadrupoles, as reported in the following table. The magnetic length L_q, the bore radius R, and the maximum gradient G_{max} (nominal for the permanent magnet types) comes from the lattice design.

Table I - DAΦNE Main Rings Quadrupole types

Type	N in 2 rings	L_q (cm)	R (cm)	L_C (cm)	R_C (cm)	R_C/L_C	G_{max} (T/m)	K_{max} (m^{-2})	Note
1- S	56	30.	5.0	30.	10.	0.333	10.	6.	Straight - Oxford
2- M	28	30.	5.4	29.2	10.6	0.363	6.	3.5	Arcs+shortKloeAnsaldo
3- L	8	40.	10.0	40.	20.	0.500	6.2	3.6	D1+FINUDA-Ansaldo
4- QF1	2	20.	5.2	20.	8.	0.400	5.93	3.49	Pm-KLOE - ASTER
5- QD	2	35.	7.3	35.	12.	0.343	9.66	5.68	Pm-KLOE - ASTER
6- QF2	2	27.	9.2	27.	16.	0.593	4.74	2.79	Pm-KLOE - ASTER
7- Q1	2	15.75	7.0	15.75	12.	0.762	9.43	5.55	Pm-FINUDA-ASTER
8- Q2	2	29.5	6.5	29.5	11.	0.373	10.80	6.35	Pm-FINUDA - ASTER

Types 1, 2, 4 have been already measured at LNF[1,2,3,4]. It is possible to fit the gradient

measurements with an analytical function[5], corresponding to the gradient created by a cylindrical current distribution with quadrupolar behaviour, described by two parameters, R_c and L_c, which are the radius and the length of the cylindrical current distribution (not necessarily equal to radius and length of the real quadrupole). In table I the values of R_c and L_c are the best values from the fit on measurements for types 1, 2 and 4; for the types where no field measurements are still available L_c is equal to the design magnetic length and R_c has been extrapolated from the measured quadrupoles.

Analytical quadrupole model

The analytical function describing the longitudinal behaviour of the gradient coming from a quadrupolar cylindrical current distribution of length $L_c = 2Z_L$ and radius R_c is[5]:

$$G_{20}(z) = const\left[\frac{9}{8} f_0(t) - f_1(t) + \frac{3}{8} f_2(t)\right]_{t_{\min}}^{t_{\max}} \tag{1}$$

with

$$f_k(t) = \left(\frac{t}{\sqrt{R_c^2 + t^2}}\right)^{2k+1} \tag{2}$$

and $t_{\max} = Z_L - z$, $t_{\min} = -Z_L - z$.

The value of the *const* is determined by the integrated gradient:

$$\int_{-L}^{L} G_{20}(z)dz = B\rho KL_q \tag{3}$$

where K and L_q are the nominal strength and magnetic length of the real quadrupole which we want to fit with the analytical function.

For each quadrupole type, the function $G_{20}(z)$ has been computed for $-L < z < L$, with $L >> L_c + R_c/L_c$, for different values of K. The $2L$ long interval has been divided into N equally long parts (see Fig. 1), and for each of them the linear matrix has been computed corresponding to a quadrupole $2L/N$ long, with a gradient G_{20}^i corresponding to the average between the two values of $G_{20}(z_i)$ and $G_{20}(z_{i+1})$, being z_i and z_{i+1} the ith interval limits. Multiplying those N linear matrices, the symmetric matrix corresponding to the total interval is obtained.

At this point it is possible to check how much this total matrix differs from the corresponding rectangular model matrix defined by:

$$2L\sum_{i=1}^{N} G_{20}^i = B\rho KL_q \tag{4}$$

For simplicity all quadrupoles have been treated in the same way, using the analytical

expression of the gradient, even if for the already measured quadrupoles the measured gradient could have been used.

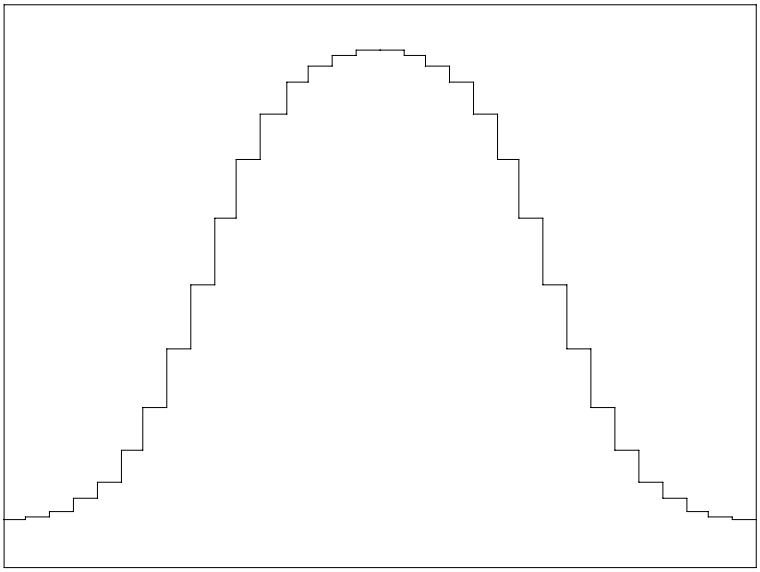

Fig. 1 *- Representation by thin rectangular matrices of the total quadrupole transport matrix*

Thin lens model

The (2×2) transport matrix describing a symmetric system in one plane has two degrees of freedom, because the two diagonal elements are equal and the matrix determinant is equal to 1. It is well known that it is possible to write the matrix as the product of two drift matrices with a thin lens in between:

$$\begin{pmatrix} a_{11} & a_{12} \\ a_{21} & a_{22} \end{pmatrix} = \begin{pmatrix} 1 & d_F \\ 0 & 1 \end{pmatrix} \begin{pmatrix} 1 & 0 \\ 1/f_F & 1 \end{pmatrix} \begin{pmatrix} 1 & d_F \\ 0 & 1 \end{pmatrix} \tag{5}$$

The value of $2d_F$ does not usually correspond to the real length of the system. The other plane will be represented by:

$$\begin{pmatrix} a_{33} & a_{34} \\ a_{43} & a_{44} \end{pmatrix} = \begin{pmatrix} 1 & d_D \\ 0 & 1 \end{pmatrix} \begin{pmatrix} 1 & 0 \\ 1/f_D & 1 \end{pmatrix} \begin{pmatrix} 1 & d_D \\ 0 & 1 \end{pmatrix} \tag{6}$$

The two parameters describing the system in one plane are then:

$$\begin{aligned} \frac{1}{f_F} &= a_{21} \\ d_F &= \frac{a_{11}-1}{a_{21}} \end{aligned} \tag{7}$$

and analogous expressions for the other plane.

The subscripts 'F' and 'D' have been chosen as referring to focusing and defocusing, because in the case of our symmetric system consisting of a quadrupole with two adjacent drifts the lenses will have opposite signs in the two planes.

Let's make first an example with the rectangular model quadrupole: considering one typical quadrupole of DAΦNE, with total magnetic length $L_q = 0.30\ m$, the values of the four characteristic parameters have been computed as functions of *K*.

We can see (Fig. 2) that $2d_F$ is larger than the original total length *2L*, while $2d_D$ is shorter. The absolute value of the focal length is larger in the focusing plane than in the defocusing. As can be easily foreseen the differences between the two planes increase for longer quadrupoles, which are more distant from the thin lens model. It is clear that the advantage of using the rectangular model representation instead of the thin lens model is that the first one depends on two parameters, while the second on four.

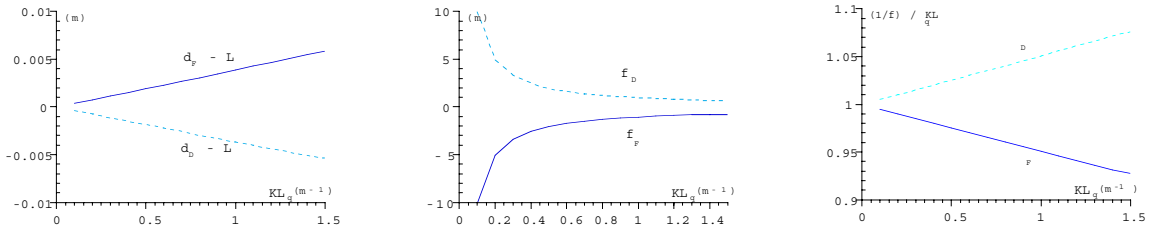

Fig. 2 *- Variation with KL_q of the four characteristic parameters in the thin lens approximation of the rectangular model quadrupole*

However the thin lens model is useful in comparing the rectangular model with the matrix obtained following the longitudinal gradient behaviour, which we will call hereon the sliced model. Applying eq. (7) to this matrix, the difference between the four characteristics parameters and the corresponding ones obtained with the rectangular model is a measure of the accuracy of the rectangular model approximation. The parameters on which this accuracy depends on are essentially two: the longitudinal shape of the gradient, which depends on the ratio R_c / L_c, and the integrated gradient value.

Figure 3 shows these fractional differences for a quadrupole with magnetic length $L_q = 0.30\ m$, versus R_c / L_c, for three different values of *K*.

It is obvious that to understand if these differences are negligible it is necessary to know the values of the betatron functions in the quadrupole position. For example in Adone it was found[6], by measuring the β functions and the machine tunes, a difference of 0.2 in the tunes of both planes with respect to the original machine model, difference which was eliminated by adjusting by ~6% the product L_qK.

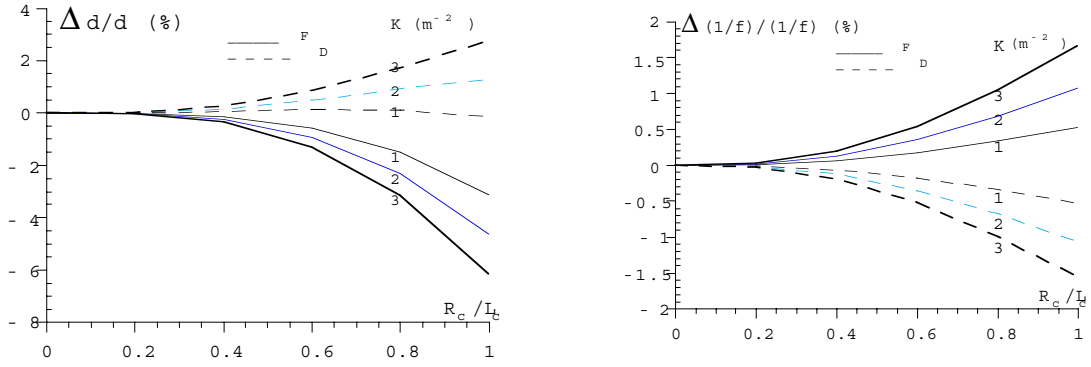

Fig. 3 *- Fractional difference in percentage of the four characteristic parameters of the sliced model with respect to those of the rectangular model versus the ratio R_C/L_C , for three different values of K for a quadrupole with L_q=0.30 m*

Constant length model

In the usual rectangular quadrupolar model of optical linear computations the actual length of the system corresponds to the model length, which is not true in the thin lens model. In general it is convenient to maintain the total length of the model equal to the real length of the system. Adding an extra parameter in the model per plane the condition on the length can be fulfilled. It is straightforward to write then the total matrix as the product of three matrices, corresponding to drift, rectangular model quadrupole and drift:

$$\begin{pmatrix} a_{11} & a_{12} \\ a_{21} & a_{22} \end{pmatrix} = \begin{pmatrix} 1 & d_F \\ 0 & 1 \end{pmatrix} \begin{pmatrix} \cos\theta_F & \dfrac{\sin\theta_F}{\sqrt{K_F}} \\ -\sqrt{K_F}\sin\theta_F & \cos\theta_F \end{pmatrix} \begin{pmatrix} 1 & d_F \\ 0 & 1 \end{pmatrix} \tag{8}$$

$$\begin{pmatrix} a_{33} & a_{34} \\ a_{43} & a_{44} \end{pmatrix} = \begin{pmatrix} 1 & d_D \\ 0 & 1 \end{pmatrix} \begin{pmatrix} \cosh\theta_D & \dfrac{\sinh\theta_D}{\sqrt{-K_D}} \\ \sqrt{-K_D}\sinh\theta_D & \cosh\theta_D \end{pmatrix} \begin{pmatrix} 1 & d_D \\ 0 & 1 \end{pmatrix} \tag{9}$$

with $\theta_F = \sqrt{K_F}\, L_{qF}$, $\theta_D = \sqrt{-K_D}\, L_{qD}$, and $L_{qD} + 2d_D = L_{qF} + 2d_F = 2L$.

From :

$$\begin{aligned} a_{11} &= \cos\theta_F - \sqrt{K_F}\; d_F \sin\theta_F \\ a_{21} &= -\sqrt{K_F}\sin\theta_F \\ a_{33} &= \cosh\theta_D + \sqrt{K_D}\; d_D \sinh\theta_D \\ a_{43} &= \sqrt{-K_D}\sinh\theta_D \end{aligned} \tag{10}$$

the values of K_F , K_D, L_{qF} and L_{qD} are determined.

We have again four parameters whose difference from the rectangular model give the measure of the accuracy of the rectangular model. Figure 4 shows an example of the fractional difference between K_F , K_D and K and between L_{qF}, L_{qD} and L_q as function of R_c / L_c for $L_q = 0.30\,m$ and $K = 2\,m^{-2}$. The magnetic length of the sliced model is shorter in the defocused plane than in the focused one, while the strength 'K' is larger in the defocused plane (in the figure the change in K refers to its absolute value).

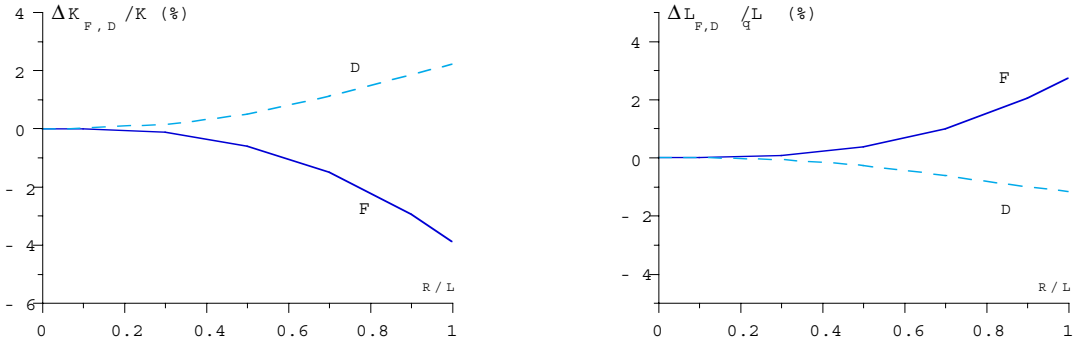

Fig. 4 *- Fractional difference between the four characteristic parameters of the sliced model and the corresponding two of the rectangular model as R_C/L_C increases for a quadrupole with $K=2.m^{-2}$ and $L_q=0.3$ m*

Normal Conducting Quadrupoles

The above considerations can be applied to DAΦNE quadrupoles. The values of the four parameters have been computed for the three different quadrupole types for values of the integrated gradient ranging from zero to the maximum value. The results are summarized in Figs. 5-7. The relative change in length and strength is in very good approximation linear with KL_q:

$$\begin{aligned} \frac{\Delta K_{F,D}}{K} &= \frac{K_{F,D} - K}{K} \approx A^K_{F,D} + C^K_{F,D}\, KL_q \\ \frac{\Delta L_{F,D}}{K} &= \frac{L_{qF,D} - L_q}{L_q} \approx A^L_{F,D} + C^L_{F,D}\, KL_q \end{aligned} \tag{11}$$

so we can write the new matrices using, instead of the nominal values of K and L_q the values obtained as:

$$\begin{aligned} K_{F,D} &= K\left(1 + A^K_{F,D} + C^K_{F,D}\, KL_q\right) \\ L_{qF,D} &= L_q\left(1 + A^L_{F,D} + C^L_{F,D}\, KL_q\right) \end{aligned} \tag{12}$$

where the coefficients $A^K_{F,D}$, $A^L_{F,D}$, $C^K_{F,D}$, $C^L_{F,D}$ are given in the following table and have been deduced by fitting the curves of Figs. 5-7. The fact that there is a term $A_{F,D}$ is due to the different behaviour of the curves very near to zero.

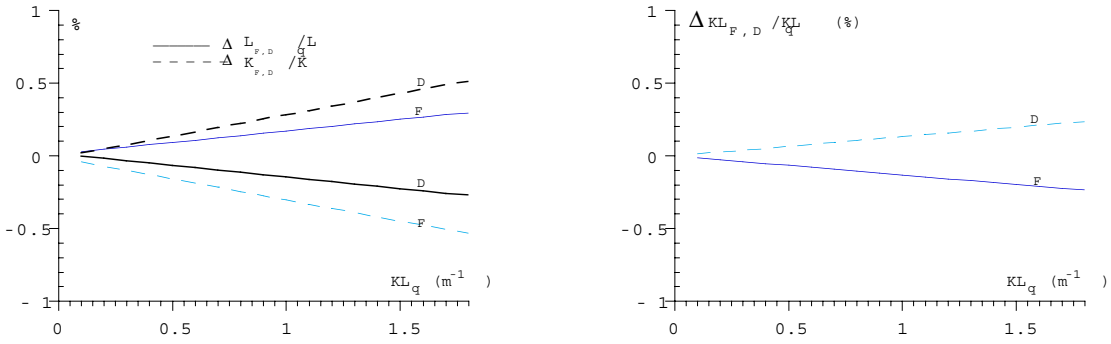

Fig. 5 - $\Delta|K|_{F,D}/|K|, \Delta L_{F,D} / L_q(a)$ *and* $\Delta|K|L_{F,D}/|K|L_q$ *(b) for the quadrupole type 1-S.*

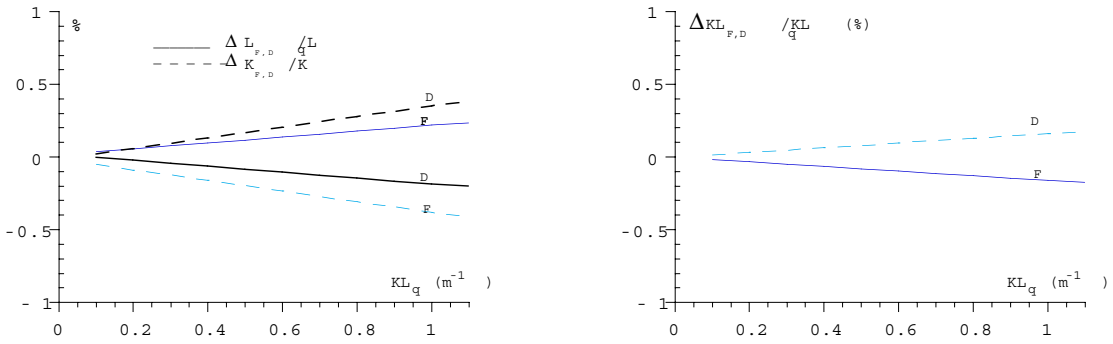

Fig. 6 - $\Delta|K|_{F,D}/|K|, \Delta L_{F,D} / L_q(a)$ *and* $\Delta|K|L_{F,D}/|K|L_q$ *(b) for the quadrupole type 2-M.*

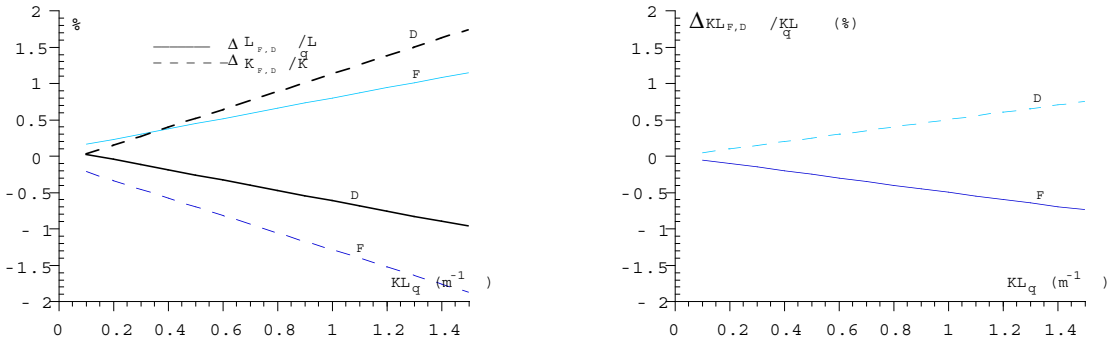

Fig. 7 - $\Delta|K|_{F,D}/|K|, \Delta L_{F,D} / L_q(a)$ *and* $\Delta|K|L_{F,D}/|K|L_q$ *(b) for the quadrupole type 3-L.*

Table II - Model Coefficients in units of 10^{-2}

Quad	A_F^K	C_F^K	A_F^L	C_F^L	A_D^K	C_D^K	A_D^L	C_D^L
1-S	-0.013	-0.290	0.013	0.160	-0.013	0.294	0.013	-0.160
2-M	-0.016	-0.362	0.016	0.203	-0.016	0.366	0.016	-0.203
3-L	-0.099	-1.186	0.093	0.708	-0.099	1.229	0.093	-0.709

Permanent Magnet Quadrupoles

There are five couples of permanent magnet quadrupoles in DAΦNE, three in the KLOE IR and two in the FI.NU.DA. one. Almost all of them have a large value for the ratio R_c/L_c, and also a high value of the gradient. Furthermore some of them are placed in the highest vertical betatron value positions, and therefore the difference between the rectangular and the sliced model cannot absolutely be neglected.

Figure 8 shows the nominal quadrupole parameters. The values of $L_{qF,D}$ and $K_{F,D}$ have been computed according to eq. (10). The differences with respect to the rectangular model values are given in Fig. 9.

Figure 10 shows the fractional difference between the nominal integrated strength and the one obtained with our model. The subscripts in these case have been named 'x' and 'y' because the polarity of the quadrupoles is fixed. All these parameters are resumed in Table III.

The accuracy of the IR optical model had been already considered[7],[8] and in fact the present nominal optics of the KLOE and FI.NU.DA IR design are based on the sliced model, which has been used to compute the integrated gradients of the pm quadrupoles.

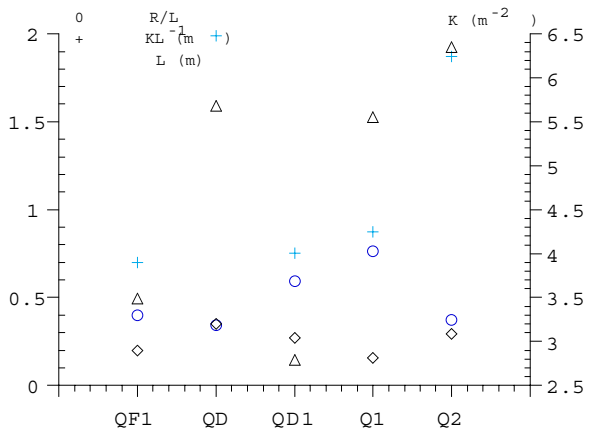

Fig. 8 *- Pm quadrupoles nominal characteristic*

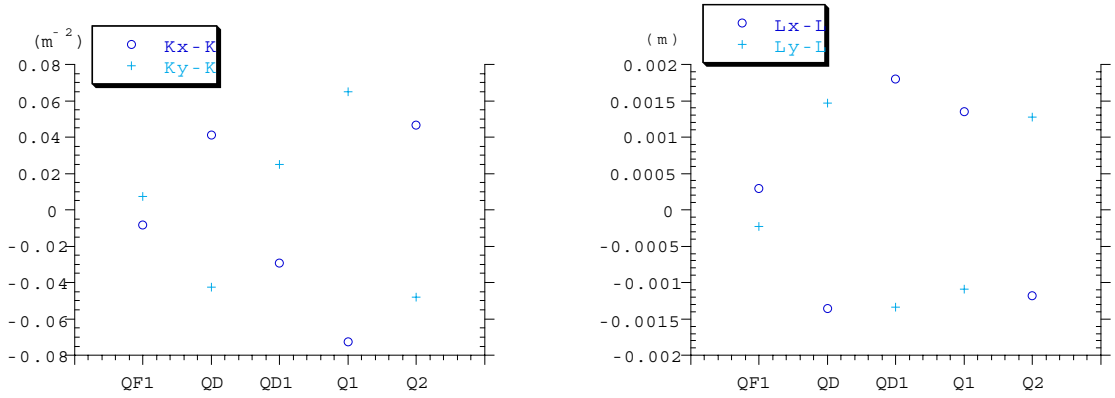

Fig. 9 *- ΔK and ΔL_q for the five types of pm quadrupoles*

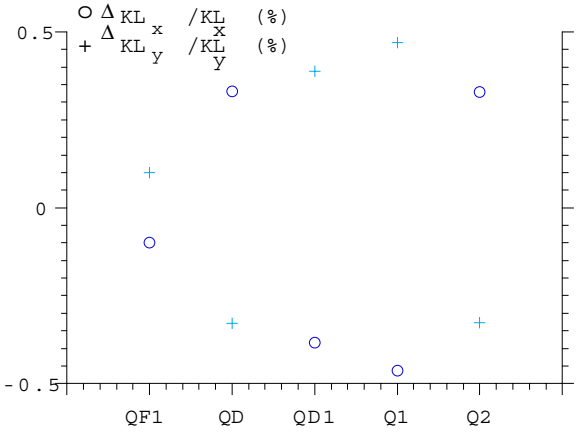

Fig. 10 *- $\left(\left|K_{x,y}\right|L_{qx,y} - |K|L_q\right)\Big/|K|L_q$ in the two planes for the permanent magnet quadrupoles*

Table III - Characteristic parameters for the permanent magnet quadrupoles

	$K_x(m^{-2})$	$K_y(m^{-2})$	$L_{qx}(m)$	$L_{qy}(m)$	$DKL_x(m^{-1})$	$DKL_y(m^{-1})$
QF1	3.4815	3.4975	0.20029	0.19977	-0.0007	0.0007
QD	5.7210	5.6377	0.34864	0.35147	0.0066	-0.0065
QF2	2.7609	2.8148	0.27180	0.26866	-0.0029	0.0029
Q1	5.4773	5.6148	0.15885	0.15641	-0.0040	0.0041
Q2	6.3965	6.3020	0.29382	0.29628	0.0062	-0.0061

Effects On The Main Ring Optics

The difference in the optical functions between a lattice calculated with the rectangular model and one calculated with the sliced model can be found by adding to each quadrupole a term ΔKL, with different sign in the two planes.

Let's remind that in a storage ring a thin lens gradient error of strength ΔKL produces in the i-th plane a tune shift given by:

$$\Delta Q_i = \frac{1}{4\pi}\beta_i \, \Delta KL \tag{13}$$

where β_i is the betatron function at the location of the gradient error. We can see for example that in the KLOE quadrupole QD where the vertical betatron function reaches ~30 m, the corresponding tune shift in the vertical plane is $\Delta Q_y = -0.016$.

The overall tune shift can be found by summing up the contributions of all quads. The total effect is always a negative tune shift: in the plane where the quadrupole focuses the value of |K| decreases and the corresponding ΔQ is negative. In the plane where the quadrupole defocuses the value of |K| increases and again ΔQ is negative. In general the effect is stronger in the plane with higher chromaticity.

In order to quantify how much the two models differ in the DAΦNE optics the DAY-ONE lattice[9] has been investigated. The rectangular model for each quadrupole has been replaced with the two matrices (8/9) obtained from the sliced model, using eqs. 12, maintaining for each quadrupole the nominal integrated gradient, and the periodic solution has been computed. The lattice parameters in the horizontal plane are shown in the following table IV.

Table IV - Difference in the ring optics due to the different quadrupole models for all quadrupoles in the horizontal plane

	Rectangular model	Sliced model
Q_x	5.090	5.057
Q_x'	-7.19	-7.35
β_x @IP (m)	4.5	4.89
α_x @IP	0.0	-0.088
D_x @IP (m)	0.0	-0.022
β_{xmax} (m)	15.32	16.12
D_{xmax} (m)	2.28	2.29
D_x (rms) (m)	1.09	1.06

In the vertical plane the tune shift is almost equal to the fractional part of the tune and the motion becomes unstable. The strongest responsible is the 3rd quadrupole of the IR where the vertical betatron function is 26 m, the integrated gradient is very high (KL_q=1.5m^{-1}) and the fringing field is long because of the quadrupole large aperture.

The difference between the two lattices has been studied also excluding the IRs, i.e., using for the IR the nominal optics and changing the quadrupole models in the arcs. The differences are summarized in the following table V. They are not negligible.

Table V - Lattice function due to the different quadrupole models for the quadrupoles in the arcs

	Rectangular model	Sliced model
Q_x	5.090	5.079
Q_x'	-7.19	-7.14
β_x @IP (m)	4.50	4.60
α_x @IP	0.00	-0.024
D_x @IP (m)	0.00	-0.015
β_{xmax} (m)	15.32	15.28
D_{xmax} (m)	2.28	2.29
D_x (rms) (m)	1.09	1.10
Q_y	6.070	6.058
Q_y'	-19.29	-20.36
β_y @IP (m)	0.045	0.042
α_y @IP	0.00	0.005
D_y @IP (m)	0.00	0.00
β_{ymax} (m)	25.73	27.56
D_{ymax} (m)	0.00	0.00
D_y (rms) (m)	0.00	0.00

We can conclude that it is convenient to take into account the field gradient behaviour all along the ring, while it is absolutely necessary in the IR design. The models will be available when all different kinds of quadrupoles will be measured. A complete description of the IR optics taking into account also the fact that the beam central trajectory is off-axis is described elsewhere[7,8].

References

[1] B. Bolli et al., "Magnetic Measurements of the first Permanent Magnet Quadrupoles (Q1) of the KLOE Interacion Region" - Technical DAΦNE Note MM-3 , Nov. 1994.

[2] B. Bolli et al., "Measurements on Tesla Quadrupole Prototype for the DAΦNE Accumulator and Main Rings" - Technical DAΦNE Note MM-4, Dic.1994.

[3] B. Bolli et al., "Field Quality and Alignment of the DAΦNE Accumulator Quadrupoles" - Technical DAΦNE Note MM-8, Ag.1995.

[4] B.Bolli et al., "Field Quality of the Small Quadrupole for the DAΦNE Main Rings" - Technical DAΦNE Note MM-10, Feb.1996.

[5] M. Bassetti and C. Biscari, "Analytical Formulae for Magnetic Multipoles" - Particle Accelerators, to be published.

[6] M. Bassetti, "Connessioni tra la funzione $\nu(k)$ e la misura dei β in Adone" Adone Memorandum T-51 (21.9.1972).

[7] C. Biscari, "Low Beta Quadrupole Fringing Field on Off-Axis Trajectory" - AIP Conference Proceedings 344, p. 88, Arcidosso, Italy 1994.

[8] M. Bassetti, C. Biscari, "Fringing Fields In Low-Beta Magnetic Elements" to be presented at EPAC 96.

[9] M.E. Biagini, C. Biscari, S. Guiducci, "DAΦNE Main Rings Lattice Update" Technical DAΦNE Note L-22 (18.3.1996).